

# Simulation of optically switchable and tunable ultrawideband monocycle generation using semiconductor optical amplifier and optical delay line

Zhefeng Hu, Junqiang Sun\*, and Jing Shao

Wuhan National Laboratory for Optoelectronics, College of Optoelectronic Science and Engineering,  
Huazhong University of Science and Technology, Wuhan, 430074, Hubei, China

## ABSTRACT

We proposed and theoretically simulated an optically switchable and tunable ultrawideband monocycle generator based on wavelength conversion in a semiconductor optical amplifier (SOA), and optical tunable delay in an optical delay line (ODL). The system is optically switchable in pulse polarity, and tunable in both pulsewidth and radio frequency (RF) spectrum.

**Keywords:** All-optical, ultrawideband (UWB), microwaves, tunability, switchability, semiconductor optical amplifier (SOA), wavelength conversion, cross-gain modulation (XGM), time delay.

## 1. INTRODUCTION

Ultrawideband (UWB) is a promising technology for short-range, high-capacity wireless communication systems and broadband sensor networks<sup>[1]</sup>. The U. S. Federal Communications Commission (FCC) has regulated the 7.5 GHz spectral band from 3.1 to 10.6 GHz for unlicensed use of UWB with a 10 dB spectral bandwidth larger than 500 MHz or a fractional bandwidth greater than 20%<sup>[2]</sup>. In the applications, UWB signal generators, which achieve pulse polarity switchability and pulsewidth or radio frequency (RF) tunability, are especially desired to provide wide applications and the flexibility of the systems.

Recently, UWB signal generation in optical domain has attracted great interests, due to the low loss over long distance transmission in the optical fiber. Both electro-optical methods<sup>[3-6]</sup> and all-optical methods<sup>[7-9]</sup> have been proposed. Particularly, Q. Wang et al. reported an ingenious scheme using cross-gain modulation (XGM) in a semiconductor optical amplifier (SOA) and time delay by two cascaded fiber Bragg gratings (FBGs)<sup>[7]</sup>. However, the FBGs should be specially designed with rigid delay and wavelength selection. Thus the wavelength can not be varied. This makes switchability and tunability very hard to realize. Electrically switchable optical UWB signal generators between monocycle and doublet pulses have been demonstrated by Q. Wang et al., but specialized polarization modulator (PolM) and polarization maintaining fiber (PMF) are required<sup>[5, 6]</sup>.

In the present paper, a novel scheme for all-optical UWB monocycle generator based on wavelength conversion in SOA and time delay in optical delay line (ODL) is proposed and simulated. The proposed scheme is optically switchable in pulse polarity, and tunable in both pulsewidth and RF spectrum.

## 2. WORKING PRINCIPLES

The operation principle of the optically switchable and tunable UWB generation scheme is shown in Fig. 1. A Gaussian pulse at  $\lambda_s$  is used as the pump signal. A continuous wave (CW) at  $\lambda_p$  is coupled with the pump signal into an SOA. Through the effect of XGM, a polarity-reversed Gaussian pulse is modulated onto the CW probe. After that, the

\*jqsun@mail.hust.edu.cn; phone: +86 27 87792242-804; fax: +86 27 87792225

Gaussian pulse and polarity-reversed Gaussian pulse are divided to different beam paths by a wavelength division multiplexer (WDM). A time delay relative to the output pump is introduced to the output probe by an ODL. By using another WDM, the output pump and probe are coupled again. Thus, the mixed signal obtains a UWB monocycle shape.

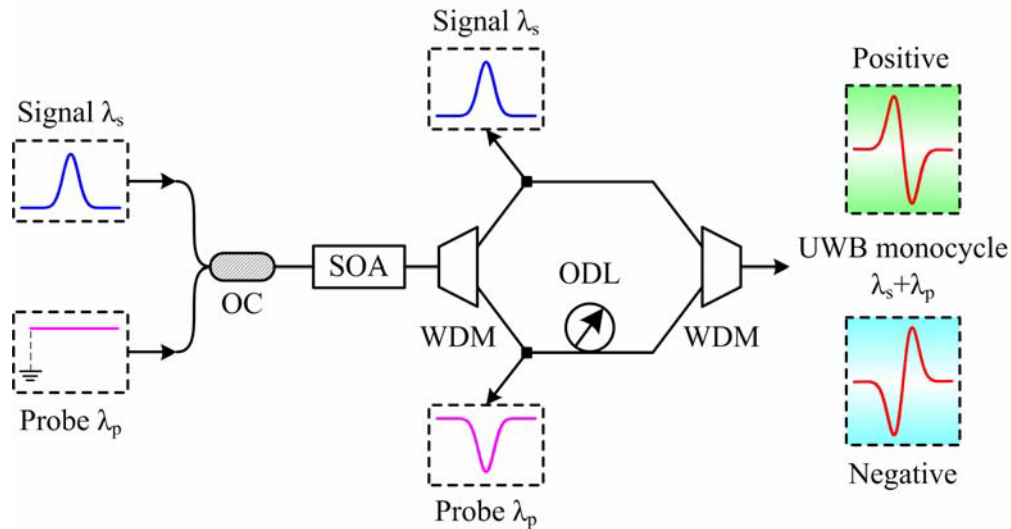


Fig. 1. Schematic illustration for the switchable and tunable UWB monocycle generator.

The time delay between the Gaussian pulse and the polarity-reversed Gaussian pulse can be controlled by tuning the ODL. Then the pulsewidth of the output UWB monocycle signal will be varied. When we tune the ODL to achieve time delay and advance, the generated pulse can be switched between positive and negative monocycle.

### 3. THEORETICAL MODELS

The XGM process in the SOA can be described by carrier rate equation and propagation equation<sup>[10]</sup>

$$\begin{cases} \frac{\partial N}{\partial t} = \frac{I}{eV} - R(N) - S_{ASE}(N) - \sum_{\omega=s,p} \frac{\Gamma g_{\omega}(N)}{A_0 hc / \lambda_{\omega}} |A_{\omega}|^2 \\ \frac{dA_{\omega}}{dz} = [\Gamma g_{\omega}(N)(1 - i\alpha) - \alpha_{int}] A_{\omega} \end{cases} \quad (1)$$

where  $N$  is the carrier density,  $I$  is the injection current,  $e$  is the quantity of electron charge,  $V$  and  $A_0$  are the volume and cross section of the active region,  $g_{\omega}(N)$  and  $hc/\lambda_{\omega}$  are the gain coefficient and the photon energy at the wavelength  $\lambda_{\omega}$  respectively, and the index  $\omega$  corresponds to different input lights, including the pump and the probe.  $R(N)$  accounts for the carrier consumption due to radiative recombination and nonradiative recombination, and  $S_{ASE}(N)$  represents the depletion due to amplified spontaneous emission (ASE) noise,  $A_{\omega}$  is the amplitudes at the wavelength  $\lambda_{\omega}$ ,  $\Gamma$  is the mode confinement factor, and  $\alpha_{int}$  is the internal loss of the SOA.

The recombination rate depends on the carrier density and is given by

$$R(N) = AN + BN^2 + CN^3 \quad (2)$$

where the coefficients  $A$ ,  $B$ , and  $C$  stand for the unimolecular recombination, bimolecular radiative recombination, and the Auger recombination process, respectively.

The gain coefficient can be expressed as

$$g_{\omega}(N, \lambda_{\omega}) = a_1(N - N_0) - a_2(\lambda_{\omega} - \lambda_N)^2 + a_3(\lambda_{\omega} - \lambda_N)^3 \quad (3)$$

where  $a_1$ ,  $a_2$ , and  $a_3$  are gain constants and  $N_0$  is the carrier density at transparency.  $\lambda_N$  is the peak wavelength, which is assumed to shift linearly with the carrier density, i.e.,  $\lambda_N = \lambda_0 - a_4(N - N_0)$ , with  $\lambda_0$  being the peak wavelength at transparency.

Here, ASE noise is ignored. Thus, we assume  $S_{ASE} = 0$ . To model the dynamic properties of the SOA, we divide it into  $m$  small segmentations. When  $m$  is large enough, the carrier density can be assumed uniform in each segment. As such, in segment  $i$ , we have

$$\begin{cases} \frac{\partial N_i}{\partial t} = \frac{I}{eV} - R(N_i) - \sum_{\omega=p,c} \frac{\Gamma g_{\omega,i}(N_i, \lambda_{\omega})}{A_0 hc / \lambda_{\omega}} |A_{\omega,i}|^2 \\ \frac{dA_{\omega,i}}{dz} = [\Gamma g_{\omega,i}(N_i, \lambda_{\omega,i})(1 - i\alpha) - \alpha_{\text{int}}] A_{\omega,i} \end{cases} \quad (4)$$

## 4. NUMERICAL SIMULATIONS

### 4.1 Simulation parameters

The simulation parameters of the SOA are listed in Table 1. The wavelength of the signal and probe are 1535 and 1550 nm respectively.

Table 1. SOA parameters.

Symbol	Description	Value
L	Length of active region	$10^{-3}$ m
w	Width of active region	$1.5 \times 10^{-6}$ m
d	Thickness of active region	$2 \times 10^{-7}$ m
A	Unimolecular recombination constant	$1.5 \times 10^8$ s <sup>-1</sup>
B	Bimolecular recombination constant	$1 \times 10^{-16}$ m <sup>3</sup> /s
C	Auger recombination constant	$1.2 \times 10^{-40}$ m <sup>6</sup> /s
$a_1$	Gain constant	$5 \times 10^{-20}$ m <sup>2</sup>
$a_2$	Gain constant	$7.4 \times 10^{18}$ m <sup>-3</sup>
$a_3$	Gain constant	$3.155 \times 10^{25}$ m <sup>-4</sup>
$a_4$	Gain constant	$3 \times 10^{-32}$ m <sup>4</sup>
$N_0$	Carrier density at transparency	$1 \times 10^{24}$ m <sup>-3</sup>
$\lambda_0$	Wavelength at transparency	$1.56 \times 10^{-6}$ m
$\alpha$	Linewidth enhancement factor	4
$\alpha_{\text{int}}$	Internal loss	$5 \times 10^3$ m <sup>-1</sup>
$\Gamma$	Confinement factor	0.3

### 4.2 Simulation results and discussions

Fig. 2 (a) shows the input Gaussian signal pulse. The full width at half maximum (FWHM) is 70 ps. The output pump and probe are shown in Fig. 2 (b) and Fig. 2 (c) respectively. The FWHMs of the output pump pulse and output probe polarity-reversed pulse are 90.7 ps and 88.1 ps respectively.

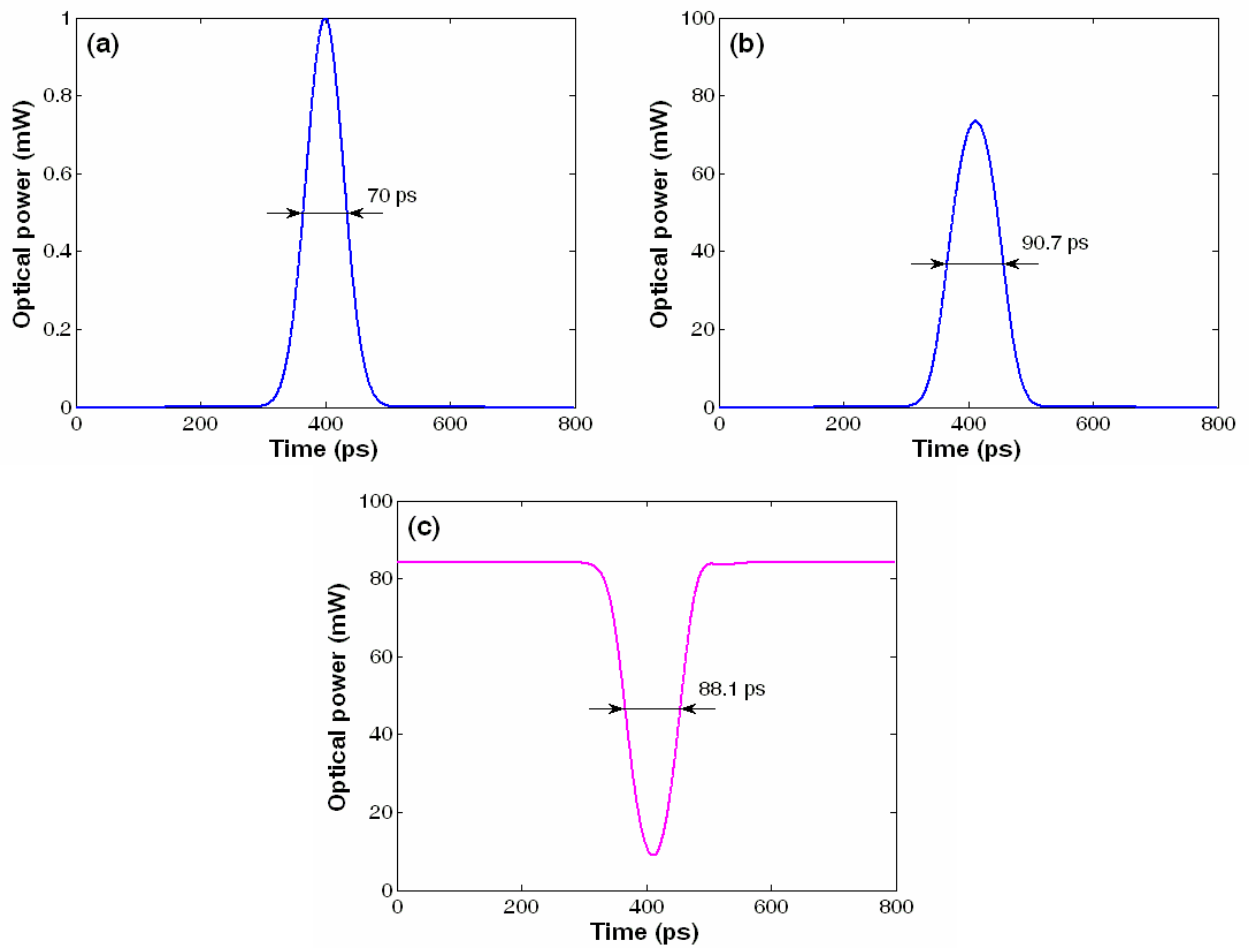


Fig. 2. Waveforms of different pulses. (a) input pump; (b) output pump; (c) output probe.

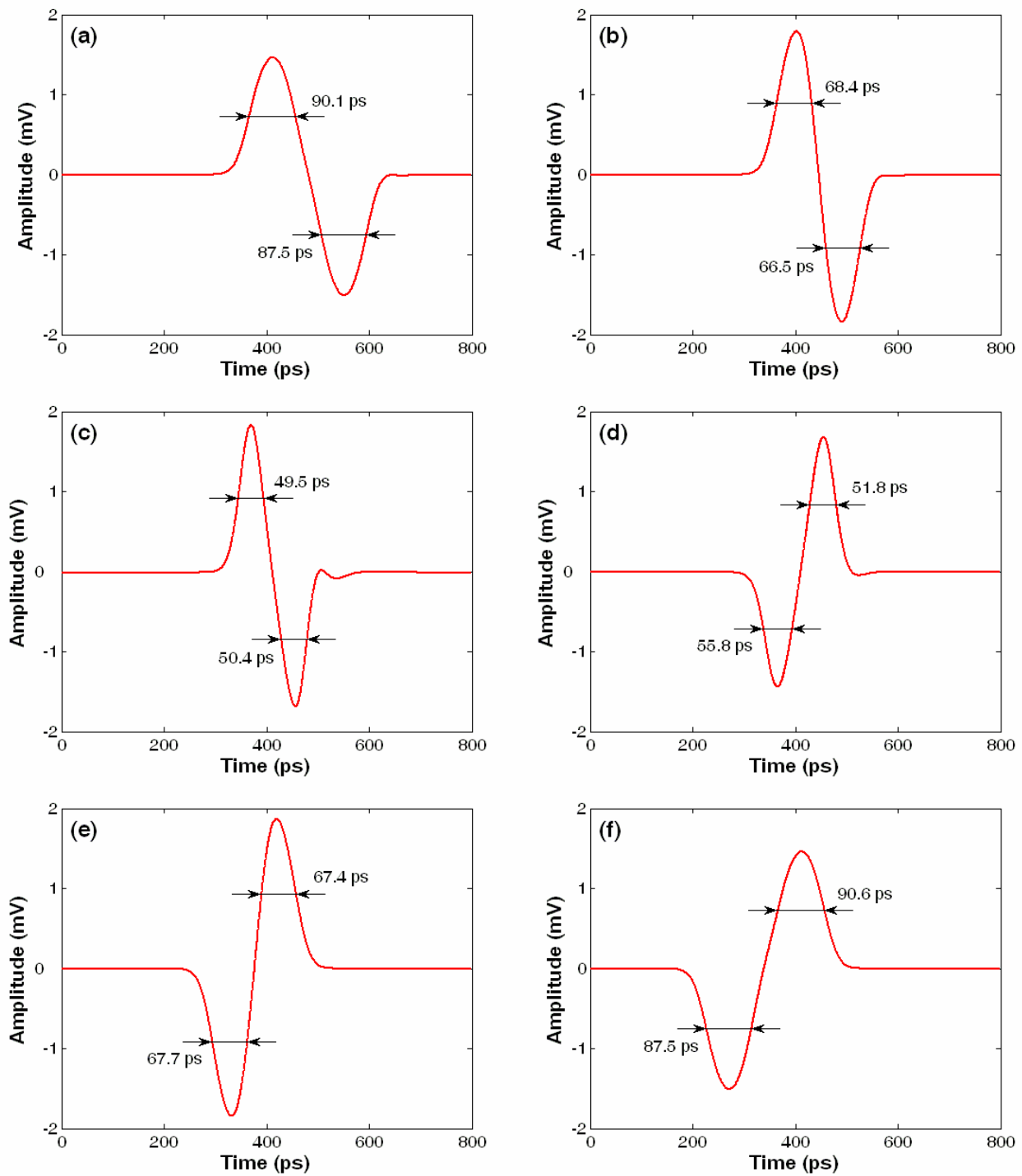


Fig. 3. Temporal trace of the generated UWB monocycle signals with different time delays [(a)-(c): 140, 70, 10 ps] and advances [(d)-(f): -10, -70, -140 ps]. (a)-(c) positive UWB monocycle; (d)-(f) negative UWB monocycle.

Fig. 3 depicts the temporal waveforms of the generated UWB monocycle, when the time delay is tuned at different values. In Fig. 3 (a)-(c), the time delays are positive. Thus, the output probe drops behind the output pump. Positive

UWB monocycle pulses are obtained. However in Fig. 3 (d)-(f), the time delays are negative. That is to say, the time advances are achieved. Then the output probe is ahead of the pump. We realize negative UWB monocycle pulses.

The dependence of the generated monocycle pulsewidth on the time delay is illustrated in Fig. 4. The negative time delays represent time advances. For the generated positive UWB monocycle signal, the upper FWHM and lower FWHM can be tuned from 49.5 to 90.1 ps and from 50.4 to 87.5 ps respectively. The corresponding parameters of the generated negative UWB monocycle signal can be tuned from 51.8 to 90.6 ps and from 55.8 to 87.5 ps respectively.

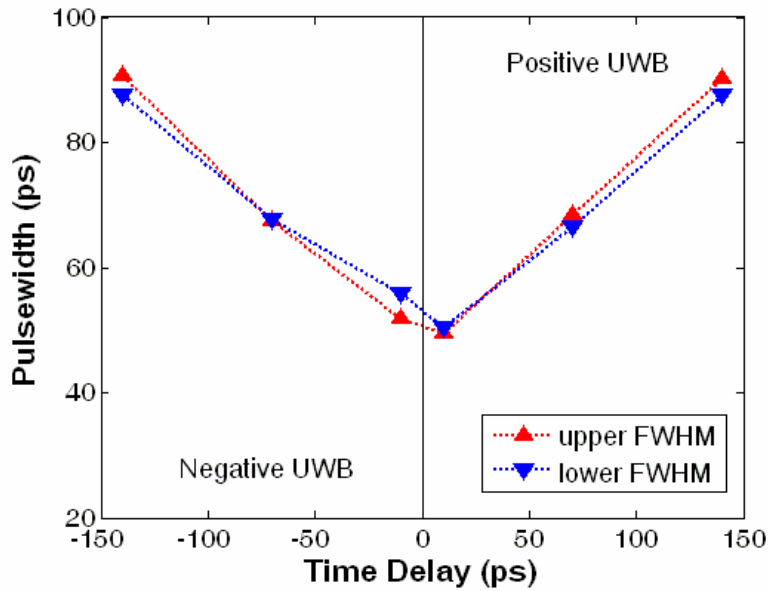


Fig. 4. Pulsewidth against the time delay.

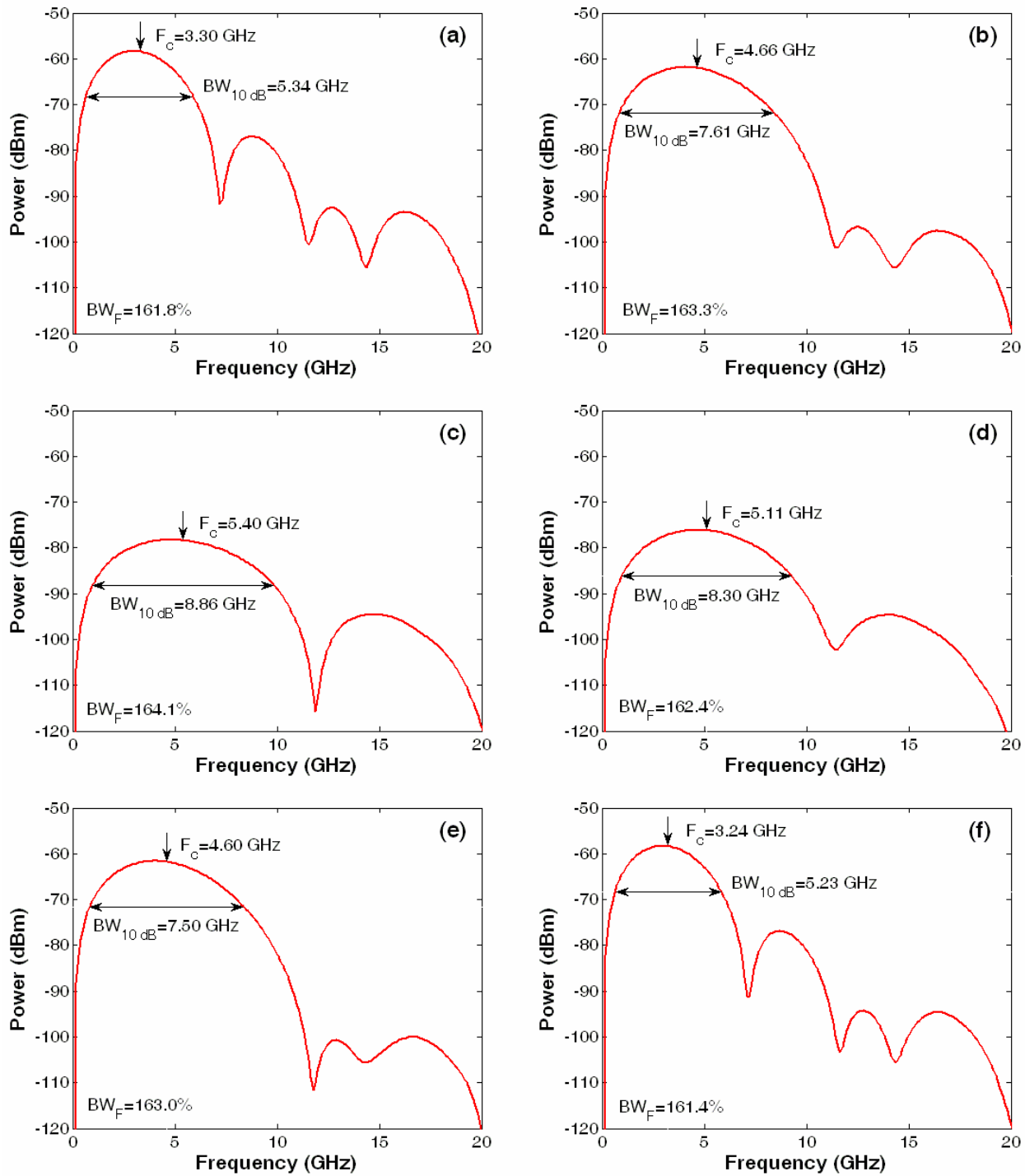


Fig. 5. Envelopes of RF spectra for UWB monocycle pulses with different time delays [(a)-(c): 140, 70, 10 ps] and advances [(d)-(f): -10, -70, -140 ps]. (a)-(c) positive UWB monocycle; (d)-(f) negative UWB monocycle.

To further confirm the successful realization of the UWB monocycle generation, Fig. 5 denotes the envelopes of the RF spectra for the generated UWB monocycle pulses. Fig. 6 plots the variation in RF spectrum when the time delay or advance is varying. From Fig. 6(a) we know that, the central frequency and 10 dB bandwidth of the generated positive

UWB monocycle can be tuned from 3.30 to 5.40 GHz and from 5.34 to 8.86 GHz respectively; and for the negative UWB monocycle, they can be tuned from 3.24 to 5.11 GHz and from 5.23 to 8.30 GHz respectively. Fig. 6(b) shows that, the fractional bandwidth of the generated monocycle signal have very slight fluctuation between 161.4% and 164.1%. It is noted that the obtained RF spectra are in good agreement with the FCC UWB definition.

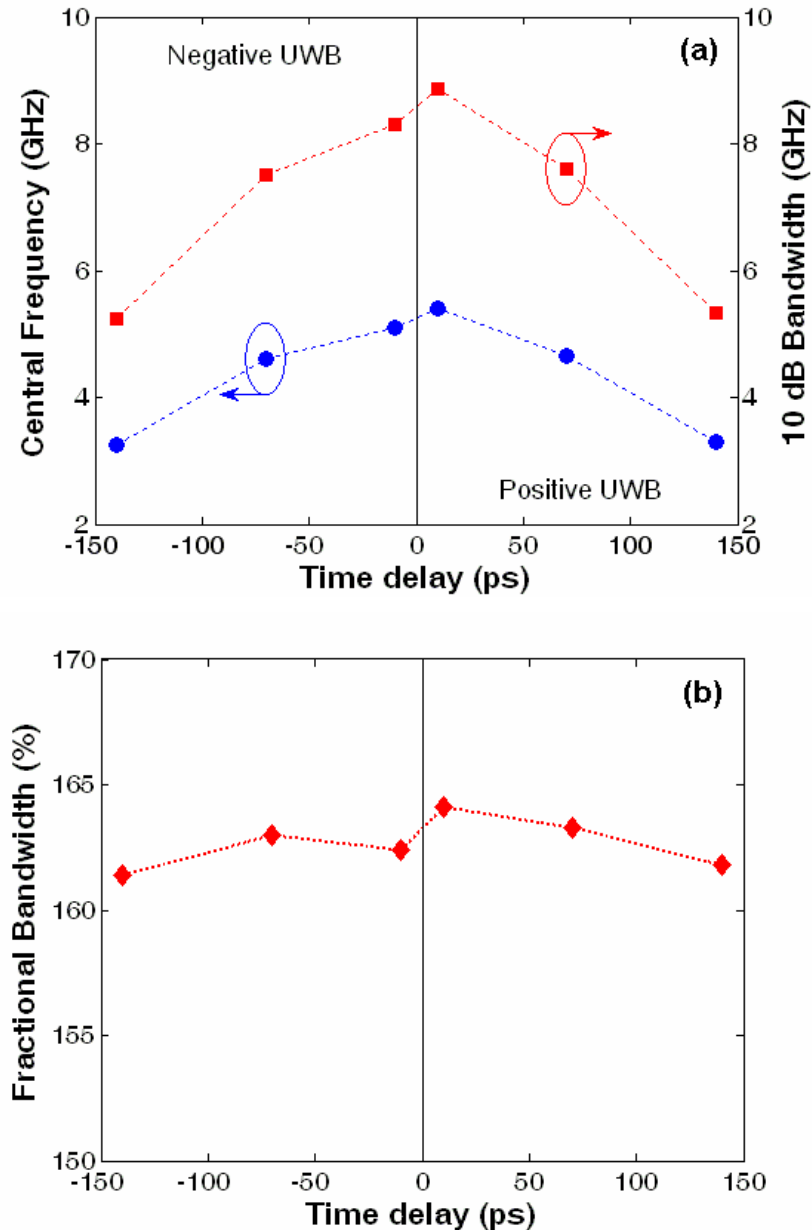


Fig. 6. (a) Central frequency, 10 dB bandwidth, and (b) fractional bandwidth as a function of the time delay.

Synthesizing the results in Fig. 3, Fig. 4, Fig. 5, and Fig. 6, we find that, when the time delay increases, the upper and lower FWHM of the generated positive UWB monocycle signal will increase, but the central frequency and 10 dB bandwidth will decrease. When the time advance increases, the upper and lower FWHM of the generated negative UWB monocycle will increase, but the central frequency and 10 dB bandwidth will decrease. Thus, we realize pulse polarity

switchability, and both pulsewidth and RF spectrum tunability for the generated UWB monocycle signal, by controlling the time delay and advance.

For the UWB signal, the pulse polarity modulation (PPM) is regarded as an important modulation scheme<sup>[11]</sup>. The proposed optically switchable monocycle generator can be expediently used for PPM for the optical UWB signal. And the optical tunability of the proposed monocycle generator offers the convenience to control the pulsewidth and the RF band for a flexible system.

## 5. CONCLUSION

We have numerically demonstrated an all-optical UWB monocycle generator. Our scheme is optically switchable in pulse polarity, and tunable in both pulsewidth and RF spectrum. The pulsewidth, central frequency and 10 dB bandwidth of the generated monocycle signal can be varied expediently by tuning the ODL. The proposed monocycle generator provides a potential method for PPM for the optical UWB signal, and also provides flexibility for the applications of UWB technology.

## ACKNOWLEDGMENTS

This work was supported by the National Natural Science Foundation of China under Grant 60678020 and Natural Science Foundation of Hubei Province of China under Grant 2008CDB313.

## REFERENCES

- [1] D. Porcine, P. Research, and W. Hirt, "Ultra-wideband radio technology: Potential and challenges ahead," *IEEE Commun. Mag.*, **41(7)**, 66-74 (2003).
- [2] G. R. Aiello and G. D. Rogerson, "Ultra-wideband wireless systems," *IEEE Microw. Mag.*, **4(2)**, 36-47 (2003).
- [3] Q. Wang and J. Yao, "UWB doublet generation using nonlinearly-biased electro-optic intensity modulator," *Electron. Lett.*, **42(22)**, 1304-1305 (2006).
- [4] F. Zeng and J. Yao, "Ultrawideband impulse radio signal generation using a high-speed electrooptic phase modulator and a fiber-Bragg-grating-based frequency discriminator," *IEEE Photon. Technol. Lett.*, **18(19)**, 2062-2064 (2006).
- [5] Q. Wang and J. Yao, "Switchable optical UWB monocycle and doublet generation using a reconfigurable photonic microwave delay-line filter," *Opt. Express*, **15(22)**, 14667-14672 (2007).
- [6] Q. Wang and J. Yao, "An electrically switchable optical ultrawideband pulse generator," *J. Lightw. Technol.*, **25(11)**, 3626-3633 (2007).
- [7] Q. Wang, F. Zeng, S. Blais, and J. Yao, "Optical ultrawideband monocycle pulse generation based on cross-gain modulation in a semiconductor optical amplifier," *Opt. Lett.*, **31(21)**, 3083-3085 (2006).
- [8] J. Dong, X. Zhang, J. Xu, and D. Huang, "Ultrawideband monocycle generation using cross-phase modulation in a semiconductor optical amplifier," *Opt. Lett.*, **32(10)**, 1223-1225 (2007).
- [9] J. Dong, X. Zhang, J. Xu, and D. Huang, "All-optical ultrawideband monocycle generation utilizing gain saturation of a dark return-to-zero signal in a semiconductor optical amplifier," *Opt. Lett.*, **32(15)**, 2158-2160 (2007).
- [10] J. Hsieh, P. Gong, S. Lee, and J. Wu, "Improved dynamic characteristics on four-wave mixing wavelength conversion in light-holding SOAs," *IEEE J. Select. Topics Quantum Electron.* **10(5)**, 1187-1196 (2004).
- [11] J. Yao, F. Zeng, and Q. Wang, "Photonic generation of ultrawideband signals," *J. Lightw. Technol.*, **25(11)**, 3219-3235 (2007).